Cardiovasc Intervent Radiol (2019) 42:260–267
https://doi.org/10.1007/s00270-018-2101-2

CLINICAL INVESTIGATION IMAGING

Visibility of Hypovascularized Liver Tumors during Intra-Arterial Therapy Using Split-Bolus Single-Phase Cone Beam CT

Martin Jonczyk[1,2] · Federico Collettini[1,2] · Dirk Schnapauff[1] · Dominik Geisel[1] · Georg Böning[1] · Willie M. Lüdemann[1] · Gero Wieners[1] · Bernd Hamm[1] · Bernhard Gebauer[1]

Received: 22 April 2018 / Accepted: 19 October 2018 / Published online: 29 October 2018

Abstract
Purpose To validate a split-bolus contrast injection protocol for single-phase CBCT in terms of detectability of hypovascular liver tumors compared to digital subtraction angiography (DSA).
Materials and Methods In this retrospective, single-center study, 20 consecutive patients with in total 77 hypovascularized tumors referred for intra-arterial therapy received a split-bolus single-phase CBCT. Two readers rated the visibility of the target tumors scheduled for embolization in CBCT and DSA compared to the pre-interventional multiphasic CT or MRI used as reference on a 3-point scoring system (1 = optimal, 3 = not visible) and catheter-associated artifacts (1 = none, 3 = extended). SNR, CNR and contrast values were derived from 37 target tumors in CBCT and MRI. Statistical analysis included the kappa test to determine interrater reliability, the Friedman's test for the inter-modality comparison evaluating tumor visibility in DSA and CBCT as well as for quantitative assessment. Post hoc analysis included the Wilcoxon signed-rank test. p values < 0.05 were considered significant.
Results Ninety percentage of target tumors were rated as visible in CBCT and 37.5% in DSA ($p < 0.001$). 70.1% of pre-interventionally detected hypovascularized tumors were depicted with CBCT and 31.2% by DSA ($p < 0.001$). 7.8% of known tumors were outside the FOV. Quantitative assessment showed higher image contrasts in CBCT (1.91 ± 7.01) compared to hepatobiliary-phase MRI (0.29 ± 0.14, $p = 0.003$) and to portal-venous (p.v.) MRI (0.31 ± 0.13, $p < 0.001$), but higher CNR for MRI (1.18 ± 0.80; 13.92 ± 15.82; 13.79 ± 6.65).
Conclusion In conclusion, the split-bolus single-phase CBCT detects significantly more hypovascularized liver tumors compared to DSA performed through the proper hepatic artery with high image contrasts.
Level of Evidence Level III, diagnostic study.

Keywords Cone beam CT · DSA · Transarterial chemoembolization · Hypovascularized · Liver tumors

Introduction

Metastases are the most common liver malignancies. Reached first by the portal-venous blood stream, especially gastrointestinal metastases tend to spread to the liver [1, 2]. Most secondary and some primary liver tumors such as the cholangiocarcinoma (CCA) present hypovascularized compared to normal liver parenchyma in the arterial and portal-venous phase throughout contrast-enhanced dynamic imaging [3, 4]. To increase diagnostic performance before therapy, contrast-enhanced magnetic resonance imaging (CE-MRI) instead of contrast-enhanced computed tomography (CE–CT) is suggested as the imaging modality of choice, which can be further increased

✉ Martin Jonczyk
martin.jonczyk@charite.de

[1] Department of Radiology, Charité – Universitätsmedizin Berlin, Freie Universität Berlin, Humboldt-Universität zu Berlin, Berlin Institute of Health, Augustenburger Platz 1, 13353 Berlin, Germany

[2] Berlin Institute of Health (BIH), Anna-Louisa-Karsch 2, 10178 Berlin, Germany

by using diffusion weighted imaging and liver-specific contrast agent such as gadolinium-ethoxybenzyl-diethylenetriamine penta-acetic acid (Gd-EOB-DTPA) [5, 6].

Intra-arterial therapies (IAT) such as transarterial embolization (TACE) and Yttrium-90 radioembolization (RE) are well-established palliative treatment options for primary and secondary liver malignancies [7–10]. However, the hypovascularized tumors are often difficult to depict during the procedure in conventional angiography [11, 12].

Cone beam CT (CBCT) proved in numerous studies its additional value in the peri-procedural setting including tumor visualization and post-embolization control [13–16]. Moreover, feeding vessel detection is facilitated through CBCT imaging [17, 18]. However, most studies concentrate on the use of CBCT in IAT for HCC [19, 20].

Schernthaner et al. [21] suggest the use of dual-phase CBCT to increase the detectability of cholangiocarcinoma compared to digital subtraction angiography (DSA) (93.4% vs. 45.9%) performing two CBCT scans after a single injection of 20 ml undiluted contrast agent with a flow rate of 2 ml/s and a delay of 3 s and 28 s. Analogous results were presented for metastatic liver disease with the same dual-phase CBCT [3]. However, split-bolus contrast injection protocols administering the contrast agent in two fractions followed by a single image acquisition have been presented for multidetector as well as cone beam CT with the aim to capture the information from two acquisitions in a single phase with subsequent reduction in radiation exposure [22–27].

The purpose of this study was to validate a split-bolus contrast injection protocol for single-phase CBCT in terms of detectability of hypovascular liver tumors compared to DSA.

Materials and Methods

In this IRB-approved, retrospective, exploratory study, 20 consecutive patients with hypovascularized tumors were included, receiving a split-bolus single-phase CBCT for IAT planning between June 2015 and May 2017. Tumors were classified as hypovascularized by their typical multiphasic pre-interventional MR or CT imaging. Hypovascular tumors were defined as liver tumors with reduced contrast uptake in arterial and portal-venous phase compared to normal liver parenchyma including hepatic metastasis from colorectal cancer, esophageal cancer and cholangiocarcinoma. All patients were referred by oncologists or surgeons for their first intra-arterial treatment. Indication for IAT was confirmed by an interdisciplinary tumor board. Institutional ethics committee approval and informed consent was obtained from all individual participants included in the study. Patients' characteristics are summarized in Table 1.

Pre-Interventional Imaging

All patients underwent pre-interventional imaging within one month before treatment receiving either multiphasic contrast-enhanced MRI or CT.

All MRI examinations were performed using a liver-specific contrast agent (Primovist® [Bayer, Germany, Leverkusen] 1 ml/10 kg body weight) in a 1.5-T MRI unit [Magnetom Avanto, Siemens Medical Solutions, Forchheim, Germany]. A dynamic T1 W VIBE sequence (TR: 4.6 ms, TE: 2.2 ms, flip angle 9°, FOV: 320 × 195 mm, pixel resolution 1.25 × 1.25 mm, slice 3 mm, NSA: 1) was performed after a predefined delay of 15 s for the arterial phase, 50 s for the portal-venous (p.v.) phase and 20 min for the hepatobiliary phase (HBP).

All multiphasic CT examinations were performed after bolus tracking for the arterial phase, 45 s for the portal-venous phase and after 90 s for the venous phase using 100 ml Ultravist 370® [Bayer, Germany, Leverkusen] on the 64 row Revolution GSI® CT [GE Healthcare, Milwaukee, USA].

Intervention

All interventions were performed by board-certified radiologists. After establishing femoral access using the Seldinger technique, DSA was performed through diagnostic catheter from the celiac trunk and the proper hepatic artery to outline hepatic artery anatomy and the main tumor feeding vessels. Catheter choice depended on patient's arterial anatomy. Either 5-F Cobra [Radiofocus® Terumo, Leuven, Belgium] or a 5-F SOS Omni Selective 3 [Soft-Vu® Angiodynamics, Queensbury, USA] or 5-F Simmons 1 catheter [Cordis, Miami Lake, USA] was used. Most DSA runs were performed with manual contrast injection and 2–3 images/s. 20 ml of contrast agent with an injection rate of 4 ml/s were injected from the truncus and the proper hepatic artery, or more selectively 10 ml of contrast agent were applied with an injection rate of 1.0–1.5 ml/s, if the injector was used.

Split-bolus single-phase CBCT was performed after positioning of the coaxial microcatheter [Cantata® 2.5F or MikroFerret-18® 3-F, Cook Medical, Bjaeversko, Denmark] in the proper hepatic artery.

In the following, all patients received either selective drug eluting beads transarterial chemoembolization with irinotecan 20 mg/ml [$N = 19$; 100 ± 25 µm Embozene TENDEM™ Microspheres, Boston Scientific, Marlborough, Massachusetts, USA] or coil embolization of the right gastric artery and the gastroduodenal artery before

Table 1 Patients' characteristics

Characteristic	Number or mean ± SD (range)
Number of patients (m/w)	20 (14/6)
Mean age (years)	66 ± 9 (51–81)
Entity (CRC/CCA/EC/Ewing Sarcoma)	14/4/1/1
Pre-interventional imaging (MRI/CT)	15/5
Pre-interventionally detected tumors	77
Mean tumor diameter (mm)	36 ± 24 (9–127)

SD standard deviation, *CRC* hepatic metastasis from colorectal cancer, *EC* hepatic metastasis from esophageal cancer, *CCA* cholangiocarcinoma

radioembolization [$N = 1$; SIRTEX®, North Sydney, NSW, Australia].

A final DSA run confirmed arterial blood flow reduction for TACE or sufficient arterial occlusion before radioembolization.

CBCT Imaging

CBCT was calibrated every day following the vendor's requirements. All contrast injection for peri-interventional CBCT were performed through microcatheters placed in the proper hepatic artery. A split-bolus injection protocol was adjusted for the intraprocedural setting for hypovascularized liver tumors. A diluted solution of Imeron® 300 [Bracco Imaging Deutschland GmbH, Konstanz, Germany] to 60% with saline was injected with the Accutron HP-D-HT® [Medtron, Saarbrücken, Germany] contrast injector. The first diluted contrast bolus of 8 ml with a flow rate of 1.5 ml/s was followed by a delay of 25 s saturates the liver parenchyma. At 30 s, a second bolus of 23 ml at the same flow rate was administered. The CBCT acquisition was initiated 38 s after the start of the first injection, respectively, 8 s after the start of the second injection. All in all, 19 ml of the diluted contrast agent was injected.

Cone beam CT was performed using the XperCT ND Roll protocol on the Allura FD20 [Philips, Best, The Netherlands] being the only available CBCT protocol allowing a lateral position of the C-arm. Rotation time was 10 s with a frame rate of 31 images/s at 120kVp, resulting in a total of 316 images per rotation. The acquired 3D volumetric CBCT images had an isotropic resolution of 0.6 mm. The flat panel detector displayed a field of view (FOV) of 250×194 mm with a matrix size of $384 \times 384 \times 296$ pixels.

Image Analysis

The qualitative assessment was performed by two board-certified radiologists (B.G. > 10 years and F.C. > 4 years of interventional experience) on all 77 pre-interventionally detected tumors. The observers could choose the window and level setting by themselves for better perception on a GE Centricity PACS workstation [GE Healthcare, Northwest Barrington, USA]. Both readers rated the visibility of the target tumors scheduled for embolization. Tumor blush and clear vascular distortion indicating a hypovascularized tumor were rated in CBCT and DSA compared to the pre-interventional multiphasic CT or MRI used as reference. A 3-point scoring system was used to describe tumor visibility (1 = optimal, 2 = suboptimal, 3 = not visible) and the appearances of catheter-associated artifacts (1 = none, 2 = circumscribed, 3 = extended). Quantitative image assessment included region of interest (ROI) measurements of each tumor, healthy liver tissue and perihepatic fat tissue for portal-venous and hepatobiliary-phase MRI as well as CBCT. SNR (S_1/S_{fat}), CNR ($|(S_{tumor}-S_{liver})/S_{fat}|$), intrinsic contrast ($C = |(S_{liver}-S_{tumor})/(S_{liver} + S_{tumor})|$) were calculated in the target tumors ($N = 37$ from 15/20 patients), whereas satellite and not displayed tumors in CBCT were omitted from the quantitative assessment. Also, patients with pre-interventional CT imaging were excluded from the quantitative analysis. The elliptical ROI measured 25 mm^2 and was placed in a representative area.

Statistical Analysis

Statistical analysis was performed using IBM SPSS Statistics 25 [Armonk, New York, USA]. The Shapiro–Wilk test was used to determine normal distribution before advanced analysis. The interrater reliability for tumor visibility in CBCT and DSA and the extension of catheter artifacts was tested with the kappa test. The Friedman's two-way analysis of variance by ranks was used for the inter-modality comparison to evaluate tumor visibility in DSA and CBCT compared to the pre-interventional imaging as well as for the quantitative assessment. Post hoc analysis was performed with the Wilcoxon signed-rank test. p values < 0.05 were considered significant.

Results

All acquired split-bolus single-phase CBCTs were performed successfully and were used for tumor segmentation and semiautomatic feeding vessel detection assisting guidance after superimposition to the real-time fluoroscopic images (Figs. 1, 2). Mean cumulative DAP in the 20 performed treatments was 256,452 ± 156,128 (70,476–479,142) mGy*cm^2 (median 191,414 mGy*cm^2). In median, two CBCTs were acquired with a mean DAP of 14,315 ± 5312 (4833–21,756) mGy*cm^2 for each CBCT (median 13,945 mGy*cm^2) meaning that in mean 7.2% of the cumulative dose was due to one CBCT acquisition. The mean cumulative CBCT DAP was 20,042 ± 16,081 (4833–60,498 mGy*cm^2) with a median of 12,079 mGy*cm^2.

Qualitative assessment revealed a significantly corresponding interrater reliability addressing image quality of patients' target tumors in DSA, whereas most hypovascularized tumors were rated as suboptimal (Reader *A*: 4 patients, Reader *B*: 7 patients) or not visible (*A*: 14 patients, *B*: 11 patients; kappa 0.346, $p = 0.038$, Table 2). Both readers independently scored the CBCT image quality equally with the best visibility in 80% and with suboptimal visibility in 10% of the patients resulting in a combined detection rate of 90% (Table 3). Only in 10% of the patients, target tumors were missed by both readers (kappa 1.000, $p < 0.001$) in CBCT, whereas in 62.5% of the patients, the target tumors were not detected in DSA (Table 3). 70.1% of the pre-interventionally detected hypovascularized tumors were depicted with CBCT and only 31.2% by DSA ($p < 0.001$, Table 3). 7.8% of tumors were missed by CBCT as they were not located in the acquired field of view. However, all tumors missed in CBCT were also not detectable in DSA. Both readers rated CBCT image quality as suboptimal in two patients because of poor CBCT start timing. Nevertheless, image quality was sufficient enough for the semiautomatic feeding vessel detection using EmboGuide (Philips Healthcare, Best, The Netherlands).

The quantitative assessment showed that portal-venous and hepatobiliary-phase MRI provides significantly higher SNR values of the liver and the tumor resulting in high CNR values (all $p < 0.001$, Table 4). However, intrinsic image contrasts are significantly higher in CBCT (1.91 ± 7.01) compared to HBP MRI: 0.29 ± 0.14, $p = 0.003$) and to p.v. MRI (0.31 ± 0.13, $p < 0.001$, Tables 4, 5).

In CBCT, the extension of distinct catheter artifacts was differently marked in the reading study ($p = 0.930$; Table 2). All catheter artifacts were found in a 2 cm radius around the diagnostic catheter positioned in the aorta and did not degrade liver imaging. Further circumscribed and extended artifacts during CBCT imaging were caused by stomach movements in 8 patients, electrocardiographic ($N = 1$) and pacemaker electrodes ($N = 1$). Moreover, hardening artifacts of the spine ($N = 3$) and through contrast agent in the vessels ($N = 2$) and kidneys' collective systems ($N = 2$) were observed. Stereotactic body radiation therapy markers ($N = 2$) and postoperative clip material

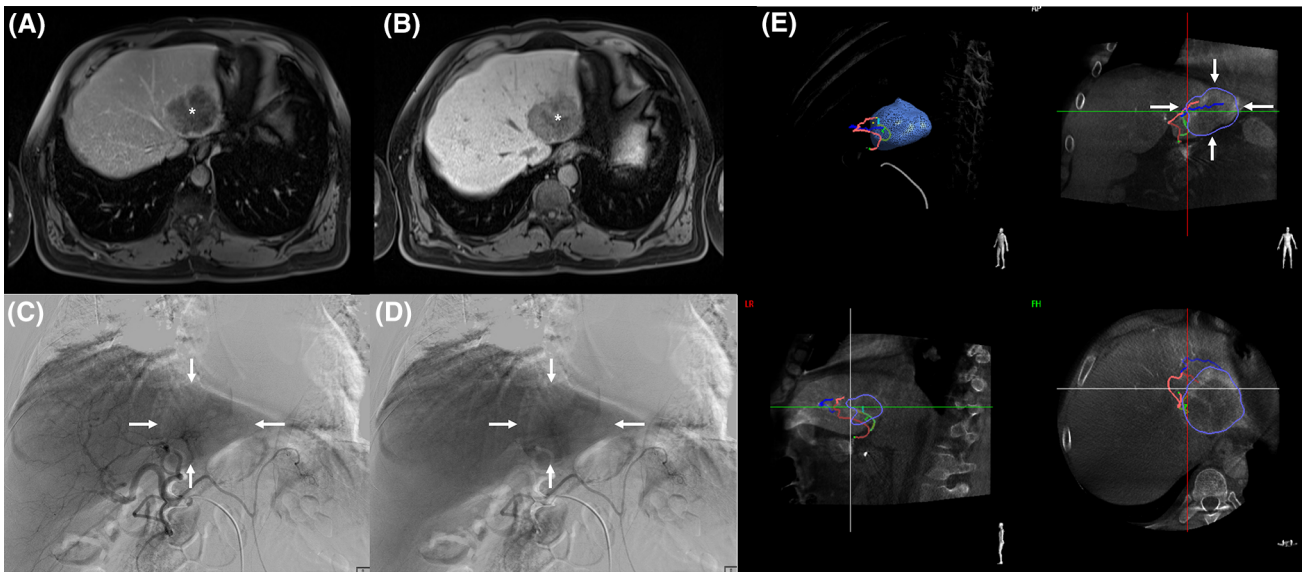

Fig. 1 **A**, **B** Portal-venous and hepatobiliary-phase MRI of a colorectal liver metastasis in the liver segment 2. **C**, **D** Early and late arterial DSA performed from the common hepatic artery, whereas reader A rated the tumor as not visible and reader B as suboptimal in DSA. Both readers agreed on optimal tumor visibility in CBCT. **E** CBCT with segmented tumor and semiautomatic feeding vessel detection. Stars and arrows indicate the target tumor

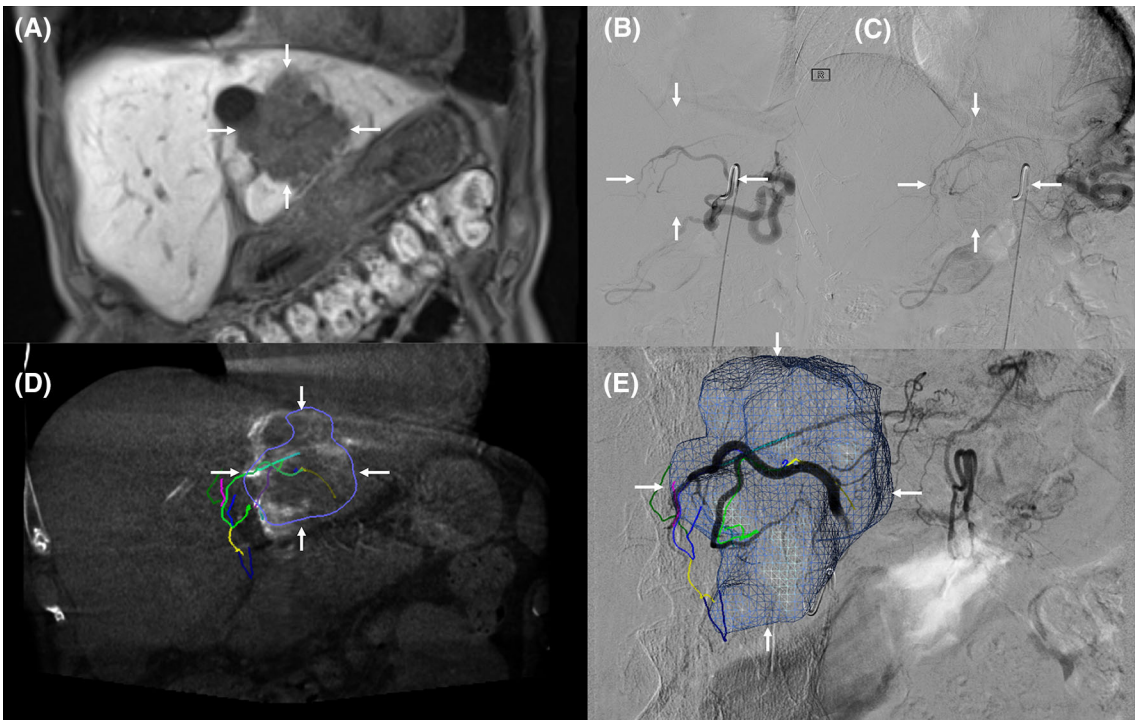

Fig. 2 **A** Hepatobiliary-phase MRI of a colorectal liver metastasis in the liver segment 2/3. **B, C** Selective early and late arterial phase DSA. Reader 1 rated tumor visibility as optimal in DSA and CBCT, whereas reader B rated the visibility in DSA with suboptimal and in CBCT with optimal. **D** Coronal CBCT reconstruction with segmented tumor and semiautomatic feeding vessel detection. **E** CBCT overlay on real-time fluoroscopy. Arrows indicate the target tumor

Table 2 Qualitative image analysis per patient and interrater reliability

	Reader *A*	Reader *B*	kappa	Significance
DSA [*N*]				
Optimal	2	2	0.346	$p = 0.038$
Suboptimal	4	7		
Not visible	14	11		
CBCT [*N*]				
Optimal	16	16	1.000	$p < 0.001$
Suboptimal	2	2		
Not visible	2	2		
Catheter artifacts [*N*]				
None	3	0	0.015	$p = 0.930$
Circumscribed	4	7		
Extended	13	13		

($N = 2$) were also accountable for noticeable artifacts in cone beam CT. Furthermore, in one case an extended ring artifact occurred around the center of the FOV. No motion artifacts due to patients' breathing occurred in the study.

Discussion

The split-bolus single-phase CBCT protocol significantly improves detection of hypovascularized tumors during intra-arterial therapy. Only 31.2% of all pre-interventionally detected tumors were visualized by DSA, whereas 70.1% were depicted with CBCT including 90% of the target tumors facilitating the procedure.

Various studies evaluated the detectability and usefulness of CBCT in TACE for HCC [19]. Miyayama et al. [28] could show that 89% of HCC could be detected in arterial phase CBCT and only 72% with DSA. Moreover, dual-phase CBCT (DP-CBCT) consisting of two CBCT rotations with an early arterial phase (EAP-CBCT) and a delayed arterial phase (DAP-CBCT) could prove even higher HCC detection rates up to 93.9% [29]. However, so far only two studies investigated the use of DP-CBCT for hypovascularized, primary and secondary liver cancers [3, 21].

Schernthaner et al. [21] could show in 17 patients that a complete tumor visualization was possible in 21.3% of DSA, 31.1% of EAP-CBCT and in 78.7% of DAP-CBCT out of 61 intrahepatic cholangiocarcinomas (CCA) compared to contrast-enhanced MRI underlining the importance of delayed contrast phase imaging. For contrast injection, the catheters were placed in the lobar hepatic

Table 3 Qualitative image analysis per tumor and inter-modality comparison DSA versus CBCT

	DSA	CBCT	
Visibility rating [*N* (%)]			$p < 0.001$
Not visible	25 (62.5)	4 (10.0)	
Suboptimal	11 (27.5)	4 (10.0)	
Optimal	4 (10.0)	32 (80.0)	
Compared to pre-interventional imaging	$p < 0.001$	$p = 0.010$	
Sub- and optimal visibility of target tumors [*N* (%)]	15 (37.5)	36 (90.0)	$p < 0.001$
Compared to pre-interventional imaging	$p < 0.001$	$p = 0.025$	
Number of tumors (%)	24/77 (31.2)	54/77 (70.1)	$p < 0.001$

Table 4 Quantitative image analysis—MRI versus CBCT

	CBCT	p.v. MRI	HBP MRI	Significance
SNR tumor	0.19 ± 2.11 (− 4.04–6.80)	18.59 ± 14.23 (4.06–74.33)	15.74 ± 7.26 (3.58–31.40)	$p < 0.001$
SNR liver	0.78 ± 1.38 (− 1.47–4.26)	32.09 ± 28.41 (2.92–173.33)	29.53 ± 11.27 (8.12–54.08)	$p < 0.001$
|CNR|	1.18 ± 0.80 (0.25–4.23)	13.92 ± 15.82 (0.20–99.00)	13.79 ± 6.65 (3.06–26.80)	$p < 0.001$
|Contrast|	1.91 ± 7.01 (0.08–43.00)	0.29 ± 0.14 (0.01–0.58)	0.31 ± 0.13 (0.09–0.60)	$p = 0.005$

Quantitative image analysis and comparison of $N = 37$ target tumors. Mean ± SD (range)

Table 5 Subgroup analysis—p.v. and HBP MRI versus CBCT

	HBP MRI versus CBCT	p.v. MRI versus CBCT	HBP versus p.v. MRI
|CNR|	$p < 0.001$	$p < 0.001$	$p = 0.202$
|Contrast|	$p = 0.003$	$p < 0.001$	$p = 0.067$

arteries. Unfortunately, feeding artery detection was not possible in DAP-CBCT demanding the EAP-CBCT.

Another study examined the visibility of neuroendocrine, colorectal and sarcoma liver metastases in DP-CBCT performed through lobar hepatic arteries and DSA compared to MRI in 28 patients [3]. Again, high rates of complete tumor detection up to 97.2% in DAP-CBCT were reported, whereas EAP-CBCT and DSA showed again lower detection rates (40.6% and 35.8%). Whereas sarcoma and colorectal cancer liver metastases appear centrally necrotic and hypovascularized with a narrow enhancing rim, neuroendocrine metastases usually present hypervascularized [30], so that this study investigated hypo- as well as hypervascularized liver metastases, which might be a reason for higher detection rates of DAP-CBCT compared to the pervious CCA study.

The advantage of the proposed split-bolus protocol is the straightforward, standardized protocol design at an early stage of the therapy through the proper hepatic artery with microcatheters. The acquired images carry the inherent image information of early and delayed arterial phase CBCT in only one instead of two rotations with high tumor detection rates and detailed feeding vessel depiction. The combined detection rate of target tumors was 90% and comparable with the results of DP-CBCT studies. Overall 70.1% of all known hypovascularized tumors known from pre-interventional imaging could be detected during the intra-arterial procedure with CBCT increasing tumor detection compared to DSA (31.2%) significantly. DSA detection rates for hypovascularized tumors were within the limits of the previously discussed studies. In this investigation, 7.8% of all pre-interventionally known tumors were missed by CBCT as they were located outside the field of view. Previous studies reported 11–20% missed tumors due to limited FOVs. However, this issue can only be addressed by new rotation trajectories increasing overall detection rates [31].

Tacher et al. [32] summarized a wide field of CBCT applications also describing a 5–10 s DP-CBCT protocol. Schernthaner et al. used the 5 s DP-CBCT protocol in their studies focusing on hypovascularized tumors acquiring 60 images per second resulting in 312 images for each rotation [3, 21, 31]. As the dual-phase CBCT requires two rotations, all in all 624 images will be acquired. The proposed split-bolus protocol lasts 10 s, however, only 31 images per second are taken resulting in a total of 316 images.

18–60 ml of contrast agent should be administered for DP-CBCT imaging [32], whereas a 60% solution of diluted

contrast agent (19 ml contrast agent and 12 ml saline) is required for split-bolus imaging which is comparable to the lowest contrast volume in the proposed DP-CBCT. Performing the split-bolus protocol with a 5 s rotation protocol would increase the delay between the injections by 5 s to a total of 30 s and decrease the amount of contrast solution for the second injection by 7–16 ml, so that a theoretical reduction in contrast agent to 15 ml would be possible to achieve a comparable contrast as with a 10-s protocol.

Schernthaner et al. [33] reported in detail the radiation exposures for the 5-s DP-CBCT protocol on an Allura FD 20 and on a Clarity angiography system [both, Philips, Best, The Netherlands]. In detail the Clarity required a median DAP of 14,000 (4700–21,200) mGy*cm^2 and the Allura FD 20 required in median DAP of 16,500 (5200–22,800) mGy*cm^2 for each CBCT acquisition which is higher for both systems compared to our proposed 10-s split-bolus CBCT protocol resulting in a median DAP of 13,945 mGy*cm^2 for each CBCT. As two rotations are required for dual-phase CBCT, the reported median cumulative CBCT DAP was 30,500 (0–103,700) mGy*cm^2 for the Clarity system and 44,800 (0–82,400) mGy*cm^2 for the Allura FD 20. Using the split-bolus protocol, considerable dose savings can be achieved as the median cumulative CBCT DAP in this study was only 12,079 mGy*cm^2.

Subgroup analysis revealed higher intrinsic contrast values of CBCT compared to MRI (Table 5). However, taking the higher spatial image resolution of CBCT images into account, SNR and CNR values were much higher for MRI with considerably less background noise (Table 4). Nevertheless, sufficient image contrast could be obtained with the split-bolus injection. On the other hand, CBCT image quality was degraded by artifacts mainly caused by catheters in this study (Table 2). However, liver tumor detection was not influenced by this finding. Nor, motion artifacts due to breathing during the 10-s scan were observed.

Whereas CBCT in TACE is an established imaging modality, only a few studies were performed concerning radioembolization [14]. Initial studies showed that CBCT can be used for macro- and microvascular assessment during radioembolization [34, 35]. The split-bolus protocol could also be used for tumor detection and selective vascular territory delineation in just one acquisition circle. Recently, Derbel et al. [36] reported that DP-CBCT can be used for virtual parenchymal perfusion studies being a promising upcoming technique for embolization territory assessment.

This study is limited by the small number of enrolled patients. Nevertheless, 77 tumors could be analyzed. Moreover, heterogeneous tumor entities were included, but all entities presented corresponding to their tumor biology hypovascularized in imaging. In future, larger studies should confirm these findings in a collective with the same intra-arterial procedure and tumor entity. Furthermore, the split-bolus protocol should be prospectively compared to the dual-phase CBCT. Moreover, not all patients had the same reference imaging for the qualitative image analysis (MRI = 15, CT = 5), however, both modalities were sufficient enough to describe patients' tumor burden.

In conclusion, the split-bolus single-phase CBCT detects significantly more hypovascularized liver tumors compared to DSA performed through the proper hepatic artery with high image contrasts.

Acknowledgements Dr. Martin Jonczyk and Dr. Federico Collettini participate in the BIH-Charité Clinical Scientist Program (DM.BIH-04.15) funded by the Charité – Universitätsmedizin Berlin and the Berlin Institute of Health.

Compliance with Ethical Standards

Conflicts of interests MJ reports Grants from BIH Clinical Scientist and Philips Healthcare during the conduct of the study; DG reports personal fees from Bayer AG during the conduct of the study; BH reports Grants from Philips Healthcare, Bayer AG, GE, Siemens and Terumo during the conduct of the study. All other authors have nothing to disclose in relation to this article.

Ethical Approval All procedures performed in studies involving human participants were in accordance with the ethical standards of the institutional and/or national research committee and with the 1964 Declaration of Helsinki and its later amendments or comparable ethical standards.

Informed Consent Informed consent was obtained from all individual participants included in the study.

References

1. Zech CJ, Herrmann KA, Reiser MF, Schoenberg SO. MR imaging in patients with suspected liver metastases: value of liver-specific contrast agent Gd-EOB-DTPA. Magn Reson Med Sci Off J Jpn Soc Magn Res Med. 2007;6:43–52.
2. Fernandez R, Pappas SG, Bentrem DJ. Clinical features of metastatic hepatic malignancies. Cancer Treat Res. 2016;168:185–202.
3. Schernthaner RE, Haroun RR, Duran R, et al. Improved visibility of metastatic disease in the liver during intra-arterial therapy using delayed arterial phase cone-beam CT. Cardiovasc Intervent Radiol. 2016;39:1429–37.
4. Reimer P, Rummeny EJ, Daldrup HE, et al. Enhancement characteristics of liver metastases, hepatocellular carcinomas, and hemangiomas with Gd-EOB-DTPA: preliminary results with dynamic MR imaging. Eur Radiol. 1997;7:275–80.
5. Zech CJ, Korpraphong P, Huppertz A, et al. Randomized multicentre trial of gadoxetic acid-enhanced MRI versus conventional MRI or CT in the staging of colorectal cancer liver metastases. Br J Surg. 2014;101:613–21.
6. Namasivayam S, Martin DR, Saini S. Imaging of liver metastases: mRI. Cancer Imaging. 2007;7:2–9.
7. Padia SA, Lewandowski RJ, Johnson GE, et al. Radioembolization of hepatic malignancies: background, quality improvement

guidelines, and future directions. J Vasc Interv Radiol. 2017; 28:1–15.
8. Gaba RC, Lewandowski RJ, Hickey R, et al. Transcatheter therapy for hepatic malignancy: standardization of terminology and reporting criteria. J Vasc Interv Radiol. 2016;27:457–73.
9. Pernot S, Artru P, Mithieux F, et al. Complete pathological response of unresectable liver metastases from colorectal cancer after trans-arterial chemoembolization with drug-eluting beads loaded with irinotecan (DEBIRI) and concomitant systemic FOLFOX: a case report from the FFCD 1201 trial. Clin Res Hepatol Gastroenterol. 2015;39:e73–7.
10. Savic LJ, Chapiro J, Geschwind JH. Intra-arterial embolotherapy for intrahepatic cholangiocarcinoma: update and future prospects. Hepatobiliary Surg Nutr. 2017;6:7–21.
11. Tognolini A, Louie JD, Hwang GL, Hofmann LV, Sze DY, Kothary N. Utility of C-arm CT in patients with hepatocellular carcinoma undergoing transhepatic arterial chemoembolization. J Vasc Interv Radiol. 2010;21:339–47.
12. Wallace MJ, Murthy R, Kamat PP, et al. Impact of C-arm CT on hepatic arterial interventions for hepatic malignancies. J Vasc Interv Radiol. 2007;18:1500–7.
13. Kakeda S, Korogi Y, Ohnari N, et al. Usefulness of cone-beam volume CT with flat panel detectors in conjunction with catheter angiography for transcatheter arterial embolization. J Vasc Interv Radiol. 2007;18:1508–16.
14. Bapst B, Lagadec M, Breguet R, Vilgrain V, Ronot M. Cone beam computed tomography (CBCT) in the field of interventional oncology of the liver. Cardiovasc Intervent Radiol. 2016;39:8–20.
15. Zheng J, Li J, Cui X, Ye H, Ye L. Comparison of diagnostic sensitivity of C-arm CT, DSA and CT in detecting small HCC. Hepatogastroenterology. 2013;60:1509–12.
16. Wang Z, Chen R, Duran R, et al. Intraprocedural 3D quantification of lipiodol deposition on cone-beam CT predicts tumor response after transarterial chemoembolization in patients with hepatocellular carcinoma. Cardiovasc Intervent Radiol. 2015;38:1548–56.
17. Miyayama S, Yamashiro M, Hattori Y, et al. Efficacy of cone-beam computed tomography during transcatheter arterial chemoembolization for hepatocellular carcinoma. Jpn J Radiol. 2011;29:371–7.
18. Miyayama S, Yamashiro M, Hashimoto M, et al. Identification of small hepatocellular carcinoma and tumor-feeding branches with cone-beam CT guidance technology during transcatheter arterial chemoembolization. J Vasc Interv Radiol. 2013;24:501–8.
19. Pung L, Ahmad M, Mueller K, et al. The role of cone-beam CT in transcatheter arterial chemoembolization for hepatocellular carcinoma: a systematic review and meta-analysis. J Vasc Interv Radiol. 2017;28:334–41.
20. Mu L, Chapiro J, Stringam J, Geschwind JF. Interventional oncology in hepatocellular carcinoma: progress through innovation. Cancer J. 2016;22:365–72.
21. Schernthaner RE, Lin M, Duran R, Chapiro J, Wang Z, Geschwind J-F. Delayed-phase cone-beam CT improves detectability of intrahepatic cholangiocarcinoma during conventional transarterial chemoembolization. Cardiovasc Intervent Radiol. 2015;38:929–36.
22. Kahn J, Kaul D, Boning G, et al. Quality and dose optimized CT trauma protocol–recommendation from a university level-I trauma center. Rofo. 2017;189:844–54.
23. Grupp U, Schafer ML, Meyer H, et al. Reducing radiation dose in emergency CT scans while maintaining equal image quality: just a promise or reality for severely injured patients? Emerg Med Int. 2013;2013:984645.
24. Brook OR, Gourtsoyianni S, Brook A, Siewert B, Kent T, Raptopoulos V. Split-bolus spectral multidetector CT of the pancreas: assessment of radiation dose and tumor conspicuity. Radiology. 2013;269:139–48.
25. Scialpi M, Palumbo B, Pierotti L, et al. Detection and characterization of focal liver lesions by split-bolus multidetector-row CT: diagnostic accuracy and radiation dose in oncologic patients. Anticancer Res. 2014;34:4335–44.
26. Scialpi M, Pierotti L, Gravante S, et al. Split-bolus multidetector-row computed tomography technique for characterization of focal liver lesions in oncologic patients. Iran J Radiol. 2016;13:e20143.
27. Jonczyk M, Chapiro J, Collettini F, et al. Diagnostic accuracy of split-bolus single-phase contrast-enhanced cone-beam CT for the detection of liver tumors before transarterial chemoembolization. J Vasc Interv Radiol. 2017;28:1378–85.
28. Miyayama S, Yamashiro M, Okuda M, et al. Usefulness of cone-beam computed tomography during ultraselective transcatheter arterial chemoembolization for small hepatocellular carcinomas that cannot be demonstrated on angiography. Cardiovasc Intervent Radiol. 2009;32:255–64.
29. Loffroy R, Lin M, Rao P, et al. Comparing the detectability of hepatocellular carcinoma by C-arm dual-phase cone-beam computed tomography during hepatic arteriography with conventional contrast-enhanced magnetic resonance imaging. Cardiovasc Intervent Radiol. 2012;35:97–104.
30. Boning G, Kahn JF, Kaul D, et al. CT follow-up in patients with neuroendocrine tumors (NETs): combined radiation and contrast dose reduction. Acta Radiol. 2018;59:517–26. https://doi.org/10.1177/0284185117726101.
31. Schernthaner RE, Chapiro J, Sahu S, et al. Feasibility of a modified cone-beam CT rotation trajectory to improve liver periphery visualization during transarterial chemoembolization. Radiology. 2015;277:833–41.
32. Tacher V, Radaelli A, Lin M, Geschwind JF. How I do it: cone-beam CT during transarterial chemoembolization for liver cancer. Radiology. 2015;274:320–34.
33. Schernthaner RE, Duran R, Chapiro J, Wang Z, Geschwind J-FH, Lin M. A new angiographic imaging platform reduces radiation exposure for patients with liver cancer treated with transarterial chemoembolization. Eur Radiol. 2015;25:3255–62.
34. Louie JD, Kothary N, Kuo WT, et al. Incorporating cone-beam CT into the treatment planning for yttrium-90 radioembolization. J Vasc Interv Radiol. 2009;20:606–13.
35. Pellerin O, Lin M, Bhagat N, Shao W, Geschwind JF. Can C-arm cone-beam CT detect a micro-embolic effect after TheraSphere radioembolization of neuroendocrine and carcinoid liver metastasis? Cancer Biother Radiopharm. 2013;28:459–65.
36. Derbel H, Kobeiter H, Pizaine G, et al. Accuracy of a cone-beam CT virtual parenchymal perfusion algorithm for liver cancer targeting during intra-arterial therapy. J Vasc Interv Radiol. 2018;29(254–61):e2.